

ScienceDirect



IFAC PapersOnLine 59-13 (2025) 165-170

Discretization based spectral submanifolds in guided car-following with time delay

Bence Szaksz*, Gábor Orosz**, and Gabor Stepan*

* Department of Applied Mechanics, Faculty of Mechanical Engineering, Budapest University of Technology and Economics, Budapest, H-1111, Hungary (e-mail: szaksz@mm.bme.hu, stepan@mm.bme.hu).

** Department of Mechanical Engineering, and Department of Civil and Environmental Engineering, University of Michigan, Ann Arbor, MI 48109, USA (e-mail: orosz@umich.edu)

Abstract: A reduced-order model based on spectral submanifolds is derived for a car-following scenario where an automated vehicle leads a human driver. The automated vehicle utilizes cruise control while also monitoring the velocity of the following vehicle, enabling itself to provide smooth guidance to the human driver. The infinite-dimensional dynamics is approximated by a large but finite-dimensional system of ordinary differential equations. Spectral submanifold calculations are then applied to extract the system's essential dynamics. The results match those obtained by delayed spectral submanifold calculations.

Copyright © 2025 The Authors. This is an open access article under the CC BY-NC-ND license (https://creativecommons.org/licenses/by-nc-nd/4.0/)

Keywords: Systems with time delays, Infinite-dimensional systems, Nonlinear model reduction, Automated vehicles, Human vehicle interaction

1. INTRODUCTION

In the literature, it is known that human-driven vehicle chains are string unstable, that is, velocity fluctuations of the leading vehicle imply increased speed fluctuations of subsequent vehicles. The development of driver assistance systems opens up the possibility of traffic control: a properly tuned automated vehicle that receives information from some connected human-driven vehicles behind/ahead, can optimize its own performance such that the surrounding vehicles also benefit. For example, it can mitigate phantom traffic jams (Molnar and Orosz, 2024), or minimize energy consumption (Shen et al., 2024).

Traffic dynamics is strongly influenced by the time delay of human drivers and that of automated vehicles, which are both in the range of 0.5–1.5 s according to the experiments in (Ge and Orosz, 2018; Ciuffo et al., 2021). The corresponding governing equations take the form of delay differential equations (DDEs), which have infinite-dimensional state space representation (Hale and Verduyn Lunel, 1993; Stepan, 1989). The analysis of the underlying dynamics is challenging, especially in the presence of relevant nonlinearities. Therefore, it is worth applying model-order reduction techniques, which can be used to identify the essential dynamics of the system.

Here, we apply the concept of spectral submanifolds (SSMs), which was introduced by Haller and Ponsioen (2016), based on the research of Haro and de la Llave (2006) and Cabré et al. (2003). The algorithm was initially proposed for ordinary differential equations (ODEs) and it was successfully applied to obtain the essential dynamics of various dynamical systems (Breunung and Haller, 2018; Jain and Haller, 2022; Opreni et al., 2023). In addition, it was generalized to the infinite-dimensional cases of partial differential equations (Kogelbauer and Haller, 2018; Buza, 2024) and delay differential equations (Szaksz et al., 2024, 2025).

In this paper, we consider the traffic scenario where an autonomous lead vehicle (AV) aims to provide smooth guidance to a subsequent human-driven vehicle (HV) (Szaksz et al., 2023b,a). While the corresponding delayed SSM calculation was carried out in (Szaksz et al., 2024), now, we discretize the governing DDE in time, and apply the SSM calculation for the corresponding high-dimensional system of ODEs. This allows one to obtain a good approximation of the system's essential dynamics without the nonlinear analysis of the intricate operator differential equations required for the exact delayed SSM calculation. This can provide a fast and reliable way to extract the essential dynamics of infinite-dimensional dynamical systems.

The paper is organized as follows. In Sec. 2, the carfollowing scenario is introduced taking into account the nonlinearities in the control of the HV. In Sec. 3, the discretization of DDEs is discussed, which is followed by the SSM calculations for one- and two-dimensional spectral subspaces in Sec. 4. Finally, we discuss the results and future goals in Sec. 5.

^{*} The research reported in this paper has been supported by the Hungarian National Research, Development and Innovation Office (NKFI-KKP-133846). The work of BSz was partially supported by the MTA-BME Lendulet "Momentum" Global Dynamics Research Group, Budapest, Hungary, while the work of GS was partially supported by the HUN-REN-BME Dynamics of Machines Research Group, Budapest, Hungary. GO acknowledges the support of the Hungarian Academy of Sciences within the Distinguished Guest Fellowship Programme and the support of the Fulbright Foundation.

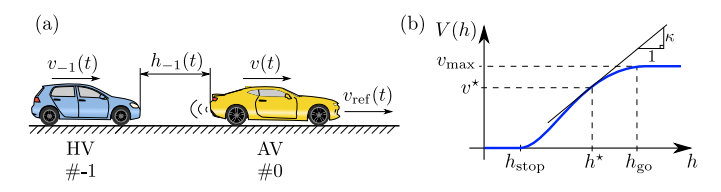


Fig. 1. Panel (a) presents the car-following model, while panel (b) shows the nonlinear range policy function of the human driver.

2. PROBLEM STATEMENT

Consider the simple car-following scenario where an automated vehicle (AV) aims to provide smooth guidance for the subsequent human-driven vehicle (HV) (see Fig. 1(a)). The velocity of the AV and that of the HV are denoted by v(t) and $v_{-1}(t)$, respectively, while the headway between the two vehicles is indicated by $h_{-1}(t)$.

Assume that the AV is equipped with a cruise control with reference velocity v_{ref} , while it also takes into account the velocity of the subsequent HV. The corresponding forward and backward looking control gains are $\hat{\beta}$ and β_{-1} .

The human driver controls the second vehicle considering the velocity difference between the two cars with the control gain β , while also taking into account the distance headway through the nonlinear range policy function $V(h_{-1})$ (see Fig. 1(b)) with the corresponding gain α .

Assuming equal time delay τ for the HV and for the AV (Ge and Orosz, 2018; Ciuffo et al., 2021), the equations of motion assume the form

$$\dot{h}_{-1}(t) = v(t) - v_{-1}(t), \tag{1}$$

$$\dot{v}_{-1}(t) = \alpha (V(h_{-1}(t-\tau)) - v_{-1}(t-\tau)) + \beta (v(t-\tau) - v_{-1}(t-\tau)),$$
(2)

$$\dot{v}(t) = \hat{\beta}(v_{\text{ref}} - v(t - \tau))
+ \beta_{-1}(v_{-1}(t - \tau) - v(t - \tau)).$$
(3)

Let us assume that the range policy function is zero for small headways $h < h_{\rm stop}$, it saturates at $v_{\rm max}$ for $h > h_{\rm go}$, while in between, it takes the form of a smooth cubic function, that is,

$$V(h) = \begin{cases} 0, & \text{if} \quad h < h_{\text{stop}}, \\ F(h), & \text{if} \quad h_{\text{stop}} \le h < h_{\text{go}}, \\ v_{\text{max}}, & \text{if} \quad h_{\text{go}} \le h, \end{cases}$$
(4)

with

$$F(h) = v_{\text{max}} \frac{(3h_{\text{go}} - h_{\text{stop}} - 2h)(h - h_{\text{stop}})^2}{(h_{\text{go}} - h_{\text{stop}})^3} \,. \tag{5}$$

In the case of steady state motion, both vehicles travel with the reference velocity $v^* = v_{\text{ref}}$, while the steady headway h^* is determined by the range policy function (5). Introducing the new variables

$$\tilde{h}_{-1} = h_{-1} - h^*, \quad \tilde{v}_{-1} = v_{-1} - v^*_{-1}, \quad \tilde{v} = v - v^*, \quad (6)$$

the corresponding state vector takes the form

$$\mathbf{x} = \begin{bmatrix} \tilde{h}_{-1} & \tilde{v}_{-1} & \tilde{v} \end{bmatrix}^{\top} . \tag{7}$$

Then, the equations of motion (1)-(3) can be written in the form of the nonlinear DDE

$$\dot{\mathbf{x}}(t) = \mathbf{A}_0 \mathbf{x}(t) + \mathbf{A}_{\tau} \mathbf{x}(t-\tau) + \mathbf{N}_{d}(\mathbf{x}(t-\tau)), \quad (8)$$

with

$$\mathbf{A}_{0} = \begin{bmatrix} 0 & -1 & 1 \\ 0 & 0 & 0 \\ 0 & 0 & 0 \end{bmatrix}, \quad \mathbf{A}_{\tau} = \begin{bmatrix} 0 & 0 & 0 \\ \alpha \kappa & -\alpha - \beta & \beta \\ 0 & \beta_{-1} & -\hat{\beta} - \beta_{-1} \end{bmatrix}, \quad (9)$$

and

$$\mathbf{N}_{\mathrm{d}}(\mathbf{\Phi}) = \frac{1}{2}\mathbf{g}_{2}(\mathbf{\Phi}, \mathbf{\Phi}) + \frac{1}{6}\mathbf{g}_{3}(\mathbf{\Phi}, \mathbf{\Phi}, \mathbf{\Phi}). \tag{10}$$

Here, the second- and third-order nonlinearities assume the forms

$$\mathbf{g}_{2}(\boldsymbol{\Phi}(-\tau), \boldsymbol{\Lambda}(-\tau)) = \begin{bmatrix} \alpha V''(h_{-1}^{\star}) \boldsymbol{\Phi}_{1}(-\tau) \boldsymbol{\Lambda}_{1}(-\tau) \\ 0 \end{bmatrix}, (11)$$

$$\mathbf{g}_{3}(\mathbf{\Phi}(-\tau), \mathbf{\Lambda}(-\tau), \mathbf{\Gamma}(-\tau)) = \begin{bmatrix} 0 \\ \alpha V'''(h_{-1}^{\star})\Phi_{1}(-\tau)\Lambda_{1}(-\tau)\Gamma_{1}(-\tau) \end{bmatrix}, \tag{12}$$

where prime denotes the derivative of the range policy function with respect to the headway and subscript 1 refers to the first component of the vectors Φ , Λ , and Γ .

The state of the DDE (8) at time t is a function of time over the interval $[t-\tau,t]$; this implies the infinite-dimensional nature of time delay systems. Here, we approximate the DDE with a large-dimensional system of ordinary differential equations (ODEs), for which the classical SSM theory can be applied (Haller and Ponsioen, 2016).

3. DISCRETIZATION OF DELAY DIFFERENTIAL EQUATIONS

There are several methods for the approximation of DDEs, which lead either to maps (Insperger and Stepan, 2011), or to a system of ODEs (Breda et al., 2016). In this paper, we consider the simplest approach, when the state of the system is sampled in an equidistant mesh of $M \geq 2$ points in $[t-\tau,t]$.

Accordingly, let us introduce the discretized state vector

$$\mathbf{y}(t) = \begin{bmatrix} \mathbf{x}(t) \\ \mathbf{x}(t + \vartheta_1) \\ \mathbf{x}(t + \vartheta_2) \\ \vdots \\ \mathbf{x}(t + \vartheta_M) \end{bmatrix}, \tag{13}$$

with the discrete time shifts $\vartheta_i = -ih$ for i = 0, 1, ..., M and $h = \tau/M$. Note that $\vartheta_0 = 0$. Introducing the notation $\mathbf{y}_i(t) = \mathbf{x}(t + \vartheta_i)$, the time derivative at the *i*-th sampling instance can be approximated with the forward Euler technique:

$$\dot{\mathbf{y}}_i(t) = \dot{\mathbf{x}}(t - ih) = \frac{\mathbf{x}(t - (i-1)h) - \mathbf{x}(t - ih)}{h}.$$
 (14)

By using the discretized state $\mathbf{y} = [\mathbf{y}_0^\top \mathbf{y}_1^\top \dots \mathbf{y}_M^\top]^\top$, the DDE (8) can be approximated with the ODE

$$\dot{\mathbf{y}}(t) = \mathbf{A}\mathbf{y}(t) + \mathbf{N}(\mathbf{y}(t)), \qquad (15)$$

where

$$\mathbf{A} = \begin{bmatrix} \mathbf{A}_0 & \mathbf{0} & \mathbf{A}_{\tau} \\ \frac{1}{h} \mathbf{I} & -\frac{1}{h} \mathbf{I} & \mathbf{0} \\ & \ddots & \ddots \\ \mathbf{0} & & \frac{1}{h} \mathbf{I} & -\frac{1}{h} \mathbf{I} \end{bmatrix}, \quad \mathbf{N}(\mathbf{y}(t)) = \begin{bmatrix} \mathbf{N}_{d}(\mathbf{y}_{M}(t)) \\ \mathbf{0} \\ \vdots \\ \mathbf{0} \end{bmatrix},$$
(16)

Here, the identity matrix is denoted by $\mathbf{I} \in \mathbb{R}^{3\times 3}$.

4. SSM CALCULATION

The matrix **A** in (16) has n = 3(M+1) eigenvalues, which we denote by λ_i (i = 1, 2, ..., n). Let us assume that all of them are in the left hand-side of the complex plane, and sort them in ascending order with respect to their real parts:

$$\operatorname{Re}\lambda_n \le \operatorname{Re}\lambda_{n-1} \le \dots \le \operatorname{Re}\lambda_2 \le \operatorname{Re}\lambda_1 < 0$$
. (17)

Note that the dominant ones approximate the relevant eigenvalues of the original DDE, while some of them are phantom roots resulting from the discretization. The exclusion of these phantom roots is not in the scope of the current paper since they do not influence the main results.

One can select the first $m \in \mathbb{N}^+$ dominant eigenvalues and calculate the corresponding eigenvectors \mathbf{v}_i , $i = 1, \dots, m$; these span the relevant tangent subspace

$$E = \operatorname{span}\{\mathbf{v}_1, \mathbf{v}_2, \dots, \mathbf{v}_m\}, \qquad (18)$$

at the origin, for which the SSM calculation is carried out.

In addition, we introduce the absolute spectral quotient

$$\Sigma(E) = \operatorname{Int}\left(\frac{\min_{\lambda \in \operatorname{Spect}(\mathbf{A})} \operatorname{Re}\lambda}{\max_{\lambda \in \operatorname{Spect}(\mathbf{A}|_{E})} \operatorname{Re}\lambda}\right), \tag{19}$$

which in our case simplifies to $\Sigma(E) = \operatorname{Int}(\operatorname{Re}\lambda_n/\operatorname{Re}\lambda_1)$.

Then, Theorem 3 in (Haller and Ponsioen, 2016) states that under the non-resonance conditions

$$\sum_{i=1}^{m} k_i \lambda_i \neq \lambda_j, \quad j = m+1, \dots, n, \quad 2 \leq \sum_{i=1}^{m} k_i \leq \Sigma(E),$$
(20)

for $k_i \in \mathbb{N}$, there exists a unique smoothest invariant manifold tangent to the spectral subspace E at the fixed point $\mathbf{y} = 0$. Close to the fixed point, this so-called spectral submanifold (SSM) $\mathbf{W} : \mathbb{C}^m \to \mathbb{R}^n$ can be represented as a polynomial in the parametrization variable $\boldsymbol{\eta} = [\eta_1, \eta_2, \dots, \eta_m]^\top$:

$$\mathbf{W}(\boldsymbol{\eta}) = \sum_{\mathbf{k}, |\mathbf{k}| \ge 1} \mathbf{W}_{\mathbf{k}} \boldsymbol{\eta}^{\mathbf{k}}, \qquad (21)$$

with the notations $\mathbf{W}_{\mathbf{k}} \in \mathbb{C}^n$, $\boldsymbol{\eta}^{\mathbf{k}} = \eta_1^{k_1} \eta_2^{k_2} \cdot \dots \cdot \eta_m^{k_m} \in \mathbb{C}$, $\mathbf{k} = [k_1, k_2, \dots, k_m]$ and $|\mathbf{k}| = k_1 + k_2 + \dots + k_m$.

The dynamics on the SSM is governed by

$$\dot{\boldsymbol{\eta}} = \mathbf{R}(\boldsymbol{\eta}) \,, \tag{22}$$

the right-hand-side $\mathbf{R}: \mathbb{C}^m \to \mathbb{C}^m$ of which can again be approximated as a polynomial in the parametrization variable, i.e.,

$$\mathbf{R}(\boldsymbol{\eta}) = \sum_{\mathbf{k}, |\mathbf{k}| \ge 1} \mathbf{R}_{\mathbf{k}} \boldsymbol{\eta}^{\mathbf{k}}, \qquad (23)$$

where $\mathbf{R}_{\mathbf{k}} \in \mathbb{C}^m$. Then, substituting $\mathbf{x}(t) = \mathbf{W}(\boldsymbol{\eta}(t))$ into the ODE (15) yields the homological equation

$$(D\mathbf{W})\mathbf{R} = \mathbf{A}\mathbf{W} + \mathbf{N}(\mathbf{W}), \qquad (24)$$

where D refers to the differential operator, such that,

$$D\mathbf{W} = [\partial \mathbf{W}/\partial \eta_1 \ \partial \mathbf{W}/\partial \eta_2 \ \dots \ \partial \mathbf{W}/\partial \eta_m]$$
. (25) Finally, the coefficients of the SSM and those of the reduced dynamics are determined by applying polynomial balance in the parametrization variables.

4.1 Treatment of nonlinearities

For the easier treatment of the nonlinearities, let us separate them into second and third order terms:

$$\mathbf{N}(\mathbf{\Phi}) = \frac{1}{2!} \mathbf{b}(\mathbf{\Phi}, \mathbf{\Phi}) + \frac{1}{3!} \mathbf{c}(\mathbf{\Phi}, \mathbf{\Phi}, \mathbf{\Phi}), \qquad (26)$$

where \mathbf{b} and \mathbf{c} are n-dimensional multilinear vectors. In case of the above discussed car-following model, these vectors take the forms

$$\mathbf{b}(\mathbf{\Phi}, \mathbf{\Lambda}) = \begin{bmatrix} \mathbf{g}_2(\mathbf{\Phi}_M, \mathbf{\Lambda}_M) \\ \mathbf{0} \\ \vdots \\ \mathbf{0} \end{bmatrix}, \tag{27}$$

$$\mathbf{c}(\mathbf{\Phi}, \mathbf{\Lambda}, \mathbf{\Gamma}) = \begin{bmatrix} \mathbf{g}_3(\mathbf{\Phi}_M, \mathbf{\Lambda}_M, \mathbf{\Gamma}_M) \\ \mathbf{0} \\ \vdots \\ \mathbf{0} \end{bmatrix}, \qquad (28)$$

where $\Phi_M, \Lambda_M, \Gamma_M \in \mathbb{C}^3$ contain the last three components of the corresponding *n*-dimensional vectors Φ, Λ, Γ , and so, they refer to the delayed state of the system.

4.2 One-dimensional reduced dynamics

Consider that λ_1 is the real dominant eigenvalue of matrix **A** such that $\text{Re}\lambda_2 < \text{Re}\lambda_1$. Then, the corresponding SSM and reduced dynamics can be approximated with

$$\mathbf{W}(\eta) = \mathbf{W}_1 \eta + \mathbf{W}_2 \eta^2 + \mathbf{W}_3 \eta^3 + \mathcal{O}(\eta^4), \qquad (29)$$

and

$$\dot{\eta} = \lambda_1 \eta + \beta_2 \eta^2 + \beta_3 \eta^3 \,, \tag{30}$$

respectively. Note that in this paper, graph-style reduced dynamics is assumed, which allows one to obtain intricate dynamics at the cost of somewhat lengthier expressions.

In this case, the homological equation (24) takes the form

$$\frac{\partial \mathbf{W}(\eta)}{\partial \eta} \dot{\eta} = \mathbf{A} \mathbf{W}(\eta) + \mathbf{N}(\mathbf{W}(\eta)), \qquad (31)$$

the expansion of which yields

$$\lambda_{1}\mathbf{W}_{1}\eta + 2\lambda_{1}\mathbf{W}_{2}\eta^{2} + \beta_{2}\mathbf{W}_{1}\eta^{2} + 3\lambda_{1}\mathbf{W}_{3}\eta^{3}$$

$$+ 2\beta_{2}\mathbf{W}_{2}\eta^{3} + \beta_{3}\mathbf{W}_{1}\eta^{3} + \mathcal{O}(\eta^{4})$$

$$= \mathbf{A}\mathbf{W}_{1}\eta + \mathbf{A}\mathbf{W}_{2}\eta^{2} + \mathbf{A}\mathbf{W}_{3}\eta^{3} + \frac{1}{2}\mathbf{b}(\mathbf{W}_{1}, \mathbf{W}_{1})\eta^{2}$$

$$+ \mathbf{b}(\mathbf{W}_{1}, \mathbf{W}_{2})\eta^{3} + \frac{1}{6}\mathbf{c}(\mathbf{W}_{1}, \mathbf{W}_{1})\eta^{3} + \mathcal{O}(\eta^{4}).$$

$$(32)$$

Applying polynomial balance for the different powers of the parametrization variable η , one obtains

$$\lambda_1 \mathbf{W}_1 = \mathbf{A} \mathbf{W}_1 \,, \tag{33}$$

$$(2\lambda_1 \mathbf{I} - \mathbf{A}) \mathbf{W}_2 = \frac{1}{2} \mathbf{b}(\mathbf{W}_1, \mathbf{W}_1) - \beta_2 \mathbf{W}_1, \qquad (34)$$

$$(3\lambda_1 \mathbf{I} - \mathbf{A})\mathbf{W}_3 = \mathbf{b}(\mathbf{W}_1, \mathbf{W}_2) + \frac{1}{6}\mathbf{c}(\mathbf{W}_1, \mathbf{W}_1, \mathbf{W}_1)$$
$$-2\beta_2 \mathbf{W}_2 - \beta_3 \mathbf{W}_1.$$
 (35)

Equation (33) is an eigenvalue-eigenvector problem implying that

$$\mathbf{W}_1 = \mathbf{v}_1 \,, \tag{36}$$

where the eigenvector \mathbf{v}_1 is defined up to a scalar multiplier. Here, the first component of \mathbf{v}_1 is selected as 1.

We should emphasize that the solution of (34) and (35) is not unique, that is, the SSM coefficients \mathbf{W}_2 and \mathbf{W}_3 depend on the selection of the reduced dynamics coefficients β_2 , β_3 . Still, as it was presented by Haller and Ponsioen (2016), although, the parametrization of the SSM is not unique, the SSM itself is.

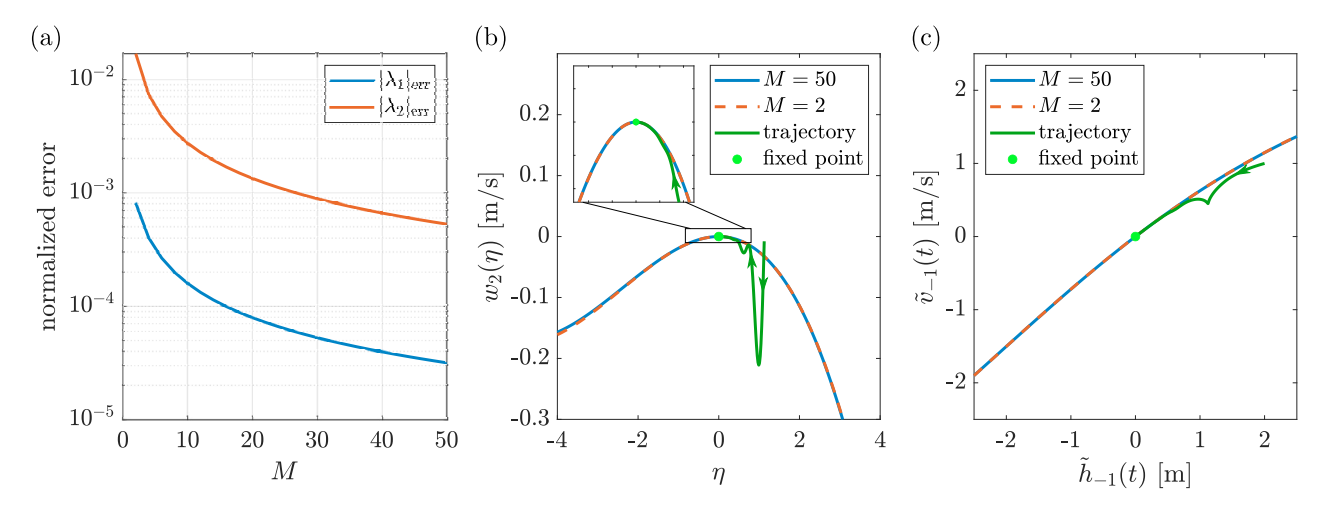


Fig. 2. Panel (a) presents the normalized error of the discretization based eigenvalues as a function of the discretization number M. Panels (b) and (c) show the convergence of a particular trajectory towards the SSM. The initial condition of the trajectory is $\tilde{v}_{-1}(t) \equiv 1 \,\text{m/s}$, $\tilde{v}(t) \equiv 0 \,\text{m/s}$, $\tilde{h}_{-1}(0) = 2 \,\text{m}$, and $\tilde{h}_{-1}(t) = \tilde{h}_{-1}(0) - \tilde{v}_{-1}(0)t$ for $t \in [-\tau, 0]$. The nonlinear part of the second coordinate of the SSM and the corresponding velocity of the HV are presented in panel (b) over the space of the parametrization variable, while in panel (c), the SSM and the trajectory are displayed in the plane of the headway and the HV's velocity.

To restrict the reduced dynamics coefficients, let us introduce the left eigenvector \mathbf{u}_1 of \mathbf{A} corresponding to the dominant eigenvalue λ_1 . Moreover, considering \mathbf{u}_1 as a row vector, apply the normalization of the left and right eigenvectors as

$$\mathbf{u}_1 \mathbf{v}_1 = 1. \tag{37}$$

Then, assume that $\mathbf{u}_1 \mathbf{W}_2 = 0$, and multiply (34) with \mathbf{u}_1 from the left. This yields that the coefficient of the second order term in the reduced dynamics takes the form

$$\beta_2 = \frac{1}{2} \mathbf{u}_1 \mathbf{b}(\mathbf{W}_1, \mathbf{W}_1). \tag{38}$$

As β_2 is already fixed, one can solve (34) for \mathbf{W}_2 under the non-resonance condition $2\lambda_1 \neq \lambda_i$, i = 2, 3, ..., n. This leads to

$$\mathbf{W}_2 = \mathbf{\Delta}^{-1}(2\lambda) \left(\frac{1}{2} \mathbf{b}(\mathbf{W}_1, \mathbf{W}_1) - \beta_2 \mathbf{W}_1 \right), \quad (39)$$

where

$$\Delta(\tilde{\lambda}) = \tilde{\lambda}\mathbf{I} - \mathbf{A} \tag{40}$$

is the characteristic matrix of the system.

Similarly, considering $\mathbf{u}_1\mathbf{W}_3=0$ and multiplying (35) with \mathbf{u}_1 from the left yields

$$\beta_3 = \mathbf{u}_1 \left(\mathbf{b}(\mathbf{W}_1, \mathbf{W}_2) + \frac{1}{6} \mathbf{c}(\mathbf{W}_1, \mathbf{W}_1, \mathbf{W}_1) \right), \quad (41)$$

and so

$$\mathbf{W}_{3} = \mathbf{\Delta}^{-1}(3\lambda) \left(\mathbf{b}(\mathbf{W}_{1}, \mathbf{W}_{2}) + \frac{1}{6} \mathbf{c}(\mathbf{W}_{1}, \mathbf{W}_{1}, \mathbf{W}_{1}) - 2\beta_{2} \mathbf{W}_{2} - \beta_{3} \mathbf{W}_{1} \right). \tag{42}$$

The SSM and the reduced dynamics coefficients can be obtained in a similar recursive manner for higher orders leading to even more accurate reduced-order models. However, this is not within the scope of the present paper.

Consider the ODE approximation of the car-following system and fix the parameters $\tau = 0.8 \,\mathrm{s}$, $\hat{\beta} = 0.15 \,\mathrm{s}^{-1}$, $\beta_{-1} = 0.3 \,\mathrm{s}^{-1}$, $\alpha = 0.3 \,\mathrm{s}^{-1}$, $\beta = 0.4 \,\mathrm{s}^{-1}$, $v_{\mathrm{max}} = 30 \,\mathrm{m/s}$,

 $v_{\rm ref}=26.55\,{\rm m/s},\ h_{\rm go}=55\,{\rm m},\ h_{\rm stop}=5\,{\rm m}.$ The exact values of the corresponding dominant eigenvalues were obtained with the semi-discretization technique (Insperger and Stepan, 2011) and a subsequent Newton-Raphson iteration yielding $\lambda_1=-0.1039$ and $\lambda_2=-0.4405$ in SI units.

Let $\lambda_{i,\text{est}}$ denote the *i*-th eigenvalue determined by the discretization discussed in Sec. 3. Figure 2(a) presents the normalized eigenvalue error $|\lambda_i|_{\text{err}} = |\lambda_{i,\text{est}} - \lambda_i|/|\lambda_i|$ as a function of the discretization variable M. As expected, the increase of M leads to a decrease in the error.

Panel (b) shows the SSM approximation and an example trajectory (obtained with the dde23 solver of MATLAB) in the plane of the parameterization variable η . Along the vertical axis, the second coordinate of the manifold is depicted, which refers to the velocity of the HV. Note that only that part of the SSM is presented, which is orthogonal to the tangent space at the fixed point. This is why w_2 is written in lowercase. In this case, even a small discretization number is enough for a reasonable approximation of the SSM.

Finally, panel (c) displays the invariant manifold and the trajectory in the plane of the headway and the velocity of the HV. In both panels (b) and (c), after a short transient, the trajectory tends to the SSM and approaches the origin along that.

4.3 Two-dimensional reduced dynamics

After the one-dimensional SSM calculation, let us present how it is carried out in a two-dimensional case. Note that the two dominant eigenvalues can either form a complex conjugate pair or both can be real.

In this case, the SSM takes the form

$$\mathbf{W} = \mathbf{W}_{10}\eta_{1} + \mathbf{W}_{01}\eta_{2} + \mathbf{W}_{20}\eta_{1}^{2} + \mathbf{W}_{11}\eta_{1}\eta_{2} + \mathbf{W}_{02}\eta_{2}^{2} + \mathbf{W}_{30}\eta_{1}^{3} + \mathbf{W}_{21}\eta_{1}^{2}\eta_{2} + \mathbf{W}_{12}\eta_{1}\eta_{2}^{2} + \mathbf{W}_{03}\eta_{2}^{3} + \mathcal{O}(\eta^{4}),$$
(43)

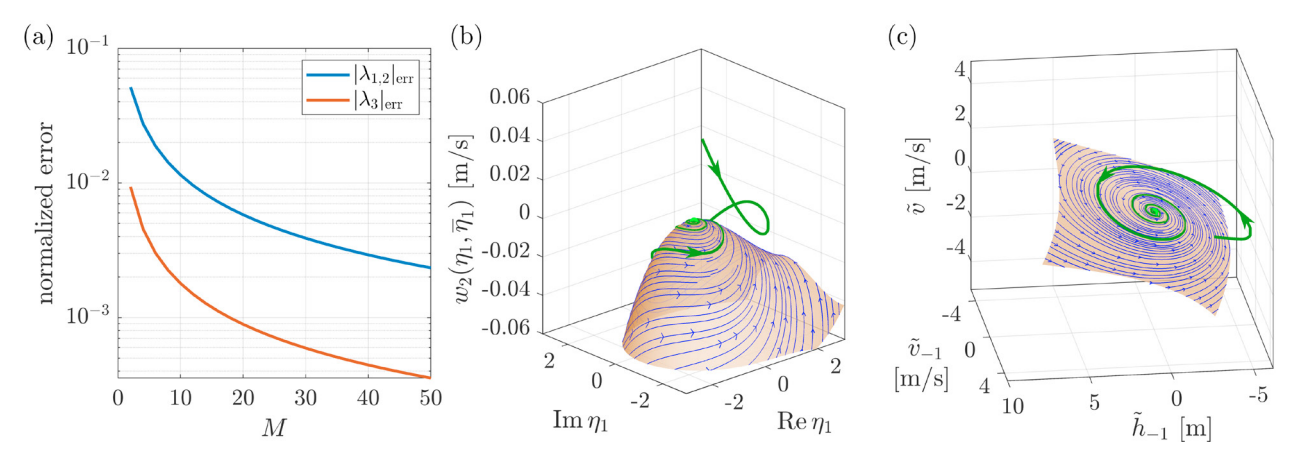


Fig. 3. Panel (a) presents the normalized error of the discretization based eigenvalues as a function of the discretization number M. Panels (b) and (c) show the convergence of a particular trajectory towards the SSM for M=30. The initial condition of the trajectory is $\tilde{v}_{-1}(t) \equiv 3\,\mathrm{m/s}$, $\tilde{v}(t) \equiv 0\,\mathrm{m/s}$, $\tilde{h}_{-1}(0) = -3\,\mathrm{m}$, and $\tilde{h}_{-1}(t) = \tilde{h}_{-1}(0) - \tilde{v}_{-1}(0)t$ for $t \in [-\tau, 0]$. The nonlinear part of the second coordinate of the SSM and the corresponding velocity of the HV are presented in panel (b) over the space spanned by the real and imaginary parts of the parametrization variable. In panel (c), the SSM and the trajectory are displayed in the space of the original state variables. The blue trajectories indicate the reduced dynamics on the SSM.

while the corresponding reduced dynamics is governed by

$$\begin{bmatrix} \dot{\eta}_1 \\ \dot{\eta}_2 \end{bmatrix} = \begin{bmatrix} \lambda_1 \eta_1 + \sum_{2 \le k+l \le 3} \beta_{kl} \eta_1^k \eta_2^l \\ \lambda_2 \eta_2 + \sum_{2 \le k+l \le 3} \gamma_{kl} \eta_1^k \eta_2^l \end{bmatrix}. \tag{44}$$

The corresponding homological equation assumes the form

$$\frac{\partial \mathbf{W}(\eta_{1}, \eta_{2})}{\partial \eta_{1}} \dot{\eta_{1}} + \frac{\partial \mathbf{W}(\eta_{1}, \eta_{2})}{\partial \eta_{2}} \dot{\eta_{2}}
= \mathbf{A} \mathbf{W}(\eta_{1}, \eta_{2}) + \mathbf{N} (\mathbf{W}(\eta_{1}, \eta_{2})),$$
(45)

which is solved again with the polynomial balance method.

The first-order terms imply that $\mathbf{W}_{10} = \mathbf{v}_1$ and $\mathbf{W}_{01} = \mathbf{v}_2$, while the second order terms yield that

$$(2\lambda_{1}\mathbf{I} - \mathbf{A})\mathbf{W}_{20} = \frac{1}{2}\mathbf{b}(\mathbf{W}_{10}, \mathbf{W}_{10}) - \beta_{20}\mathbf{W}_{10} - \gamma_{20}\mathbf{W}_{01},$$
(46)

$$((\lambda_1 + \lambda_2)\mathbf{I} - \mathbf{A})\mathbf{W}_{11} = \mathbf{b}(\mathbf{W}_{10}, \mathbf{W}_{01}) - \beta_{11}\mathbf{W}_{10} - \gamma_{11}\mathbf{W}_{01},$$
(47)

$$(2\lambda_{2}\mathbf{I} - \mathbf{A})\mathbf{W}_{02} = \frac{1}{2}\mathbf{b}(\mathbf{W}_{01}, \mathbf{W}_{01}) - \beta_{02}\mathbf{W}_{10} - \gamma_{02}\mathbf{W}_{01}.$$
(48)

Let us introduce \mathbf{u}_1 and \mathbf{u}_2 as the left eigenvectors of \mathbf{A} corresponding to λ_1 and λ_2 such that $\mathbf{u}_1\mathbf{v}_1=1$ and $\mathbf{u}_2\mathbf{v}_2=1$. Then, considering that \mathbf{W}_{20} , \mathbf{W}_{11} and \mathbf{W}_{02} are orthogonal to the left eigenvectors \mathbf{u}_1 and \mathbf{u}_2 , one obtains

$$\beta_{20} = \frac{1}{2} \mathbf{u}_1 \mathbf{b}(\mathbf{W}_{10}, \mathbf{W}_{10}), \ \gamma_{20} = \frac{1}{2} \mathbf{u}_2 \mathbf{b}(\mathbf{W}_{10}, \mathbf{W}_{10}), \ (49)$$

$$\beta_{11} = \mathbf{u}_1 \mathbf{b}(\mathbf{W}_{10}, \mathbf{W}_{01}), \quad \gamma_{11} = \mathbf{u}_2 \mathbf{b}(\mathbf{W}_{10}, \mathbf{W}_{01}), \quad (50)$$

$$\beta_{02} = \frac{1}{2} \mathbf{u}_1 \mathbf{b}(\mathbf{W}_{01}, \mathbf{W}_{01}), \ \gamma_{02} = \frac{1}{2} \mathbf{u}_2 \mathbf{b}(\mathbf{W}_{01}, \mathbf{W}_{01}).$$
 (51)

Note that here we utilized that $\mathbf{u}_1\mathbf{v}_2=0$ and $\mathbf{u}_2\mathbf{v}_1=0$ are also satisfied.

Then, under the corresponding non-resonance conditions, the second order coefficients of the SSM assume the form

$$\mathbf{W}_{20} = \mathbf{\Delta}^{-1}(2\lambda_1) \left(\frac{1}{2} \mathbf{b}(\mathbf{W}_{10}, \mathbf{W}_{10}) - \beta_{20} \mathbf{W}_{10} - \gamma_{20} \mathbf{W}_{01} \right),$$

$$(52)$$

$$\mathbf{W}_{11} = \mathbf{\Delta}^{-1}(\lambda_1 + \lambda_2) \bigg(\mathbf{b}(\mathbf{W}_{10}, \mathbf{W}_{01}) - \beta_{11} \mathbf{W}_{10} - \gamma_{11} \mathbf{W}_{01} \bigg),$$

$$(53)$$

$$\mathbf{W}_{02} = \mathbf{\Delta}^{-1}(2\lambda_2) \left(\frac{1}{2} \mathbf{b}(\mathbf{W}_{01}, \mathbf{W}_{01}) - \beta_{02} \mathbf{W}_{10} - \gamma_{02} \mathbf{W}_{01} \right).$$
(54)

The same procedure can be carried out for the third (and higher) order terms, however, this leads to lengthy expressions, which are now omitted for brevity.

If the two most dominant eigenvalues are real, then all the above coefficients are real as well. On the other hand, if the dominant eigenvalues form a complex conjugate pair, then the following symmetries are present: $\mathbf{W}_{kl} = \overline{\mathbf{W}}_{lk}$ and $\gamma_{kl} = \overline{\beta}_{lk}$ for $k+l \geq 2$. In the current paper, we consider the complex conjugate case.

Let us fix the system parameters to the same values as before, except for the control gains of the automated vehicle, which are now $\hat{\beta} = -0.4\,\mathrm{s}^{-1}$ and $\beta_{-1} = 0.6\,\mathrm{s}^{-1}$. Then, the leading eigenvalues form the complex conjugate pair $\lambda_{1,2} = -0.0885 \pm 0.6374\,\mathrm{i}$, while the third one is $\lambda_3 = -0.4448$.

Fig. 3(a) presents the normalized error of the discretization-based eigenvalues. Now, the leading eigenvalue has a larger error than the third, which can be explained by the fact that λ_1 and λ_2 form a complex conjugate pair, while λ_3 is

Panels (b) and (c) show the convergence of a trajectory to the SSM. The brown surface refers to the SSM, on which the blue trajectories are obtained via the reduced dynamics. In panel (b), the nonlinear part of the SSM is presented above the space spanned by the real and imaginary parts of the parametrization variable η_1 , while panel (c) shows the SSM and the trajectory in the space of the state variables \tilde{h}_{-1} , \tilde{v}_{-1} and \tilde{v} . It can be seen that the trajectory converges to the SSM and spirals towards the origin along a path predicted by the reduced dynamics.

5. CONCLUSION

The powerful concept of spectral submanifolds has been applied to time delay systems recently. However, the corresponding theoretical background required an intricate operator differential equations based derivation. Here, we proposed to approximate the time delay systems with a large but finite-dimensional system of ordinary differential equations and calculated the corresponding SSMs. This was inspired by the application of SSM theory to the finite element models (FEMs) of continuum structures present in the literature (Jain and Haller, 2022), which is basically a finite-dimensional approximation of an infinite-dimensional system.

The theory was applied to obtain the essential dynamics of a car-following model, where an AV aims to provide a smooth guidance to the following HV. The case studies included both the case of a dominant real eigenvalue and the case of a dominant pair of complex conjugate eigenvalues. The results show that the SSM of the system can be approximated well even with the proposed simple discretization technique. These numerical results validate the cumbersome algebraic outcome of the delayed SSM calculation (Szaksz et al., 2024, 2025).

In the future, we plan to investigate the dynamics of the system for various control parameter combinations and we also aim to consider different time delays for the HV and for the AV. This is expected to lead to more intricate dynamics, for which the discretization number must be increased.

Our final goal is to utilize the SSM and the corresponding reduced dynamics to propose an optimal control parameter setting for the AV, which takes into account the relevant nonlinearities of the system.

REFERENCES

- Breda, D., Diekmann, O., Gyllenberg, M., Scarabel, F., and Vermiglio, R. (2016). Pseudospectral discretization of nonlinear delay equations: new prospects for numerical bifurcation analysis. SIAM Journal on Applied Dynamical Systems, 15(1), 1–23.
- Breunung, T. and Haller, G. (2018). Explicit backbone curves from spectral submanifolds of forced-damped nonlinear mechanical systems. *Proceedings of the Royal Society A*, 474(2213), 20180083.
- Buza, G. (2024). Spectral submanifolds of the Navier–Stokes equations. SIAM Journal on Applied Dynamical Systems, 23(2), 1052–1089.
- Cabré, X., Fontich, E., and de la Llave, R. (2003). The parameterization method for invariant manifolds i: manifolds associated to non-resonant subspaces. *Indiana University Mathematics Journal*, 283–328.

- Ciuffo, B., Mattas, K., Makridis, M., Albano, G., Anesiadou, A., He, Y., Josvai, S., Komnos, D., Pataki, M., Vass, S., and Szalay, Z. (2021). Requiem on the positive effects of commercial adaptive cruise control on motorway traffic and recommendations for future automated driving systems. Transportation Research Part C, 130, 103305.
- Ge, J.I. and Orosz, G. (2018). Connected cruise control among human-driven vehicles: Experiment-based parameter estimation and optimal control design. *Transportation Research Part C*, 95, 445–459.
- Hale, J.K. and Verduyn Lunel, S.M. (1993). *Introduction to Functional Differential Equations*. Springer.
- Haller, G. and Ponsioen, S. (2016). Nonlinear normal modes and spectral submanifolds: existence, uniqueness and use in model reduction. *Nonlinear Dynamics*, 86(3), 1493–1534.
- Haro, A. and de la Llave, R. (2006). A parameterization method for the computation of invariant tori and their whiskers in quasi-periodic maps: rigorous results. *Jour*nal of Differential Equations, 228(2), 530–579.
- Insperger, T. and Stepan, G. (2011). Semi-discretization for Time-delay Systems. Springer.
- Jain, S. and Haller, G. (2022). How to compute invariant manifolds and their reduced dynamics in high-dimensional finite element models. *Nonlinear Dynamics*, 107(2), 1417–1450.
- Kogelbauer, F. and Haller, G. (2018). Rigorous model reduction for a damped-forced nonlinear beam model: an infinite-dimensional analysis. *Journal of Nonlinear Science*, 28, 1109–1150.
- Molnar, T.G. and Orosz, G. (2024). Destroying phantom jams with connectivity and automation: Nonlinear dynamics and control of mixed traffic. *Transportation Science*, 58(6), 1319–1334.
- Opreni, A., Vizzaccaro, A., Touzé, C., and Frangi, A. (2023). High-order direct parametrisation of invariant manifolds for model order reduction of finite element structures: application to generic forcing terms and parametrically excited systems. *Nonlinear Dynamics*, 111(6), 5401–5447.
- Shen, M., Dollar, R.A., Molnar, T.G., He, C.R., Vahidi, A., and Orosz, G. (2024). Energy-efficient reactive and predictive connected cruise control. *IEEE Transactions on Intelligent Vehicles*, 9(1), 944–957.
- Stepan, G. (1989). Retarded Dynamical Systems. Longman, Harlow.
- Szaksz, B., Orosz, G., and Stepan, G. (2023a). Nonlinear guidance of a human driver via an automated vehicle. In *IUTAM Symposium on Nonlinear Dynamics for Design of Mechanical Systems Across Different Length/Time Scales*, 405–416. Springer.
- Szaksz, B., Orosz, G., and Stepan, G. (2024). Reduction to spectral submanifolds in guided car-following with time delay. *IFAC-PapersOnLine*, 58(27), 67–72.
- Szaksz, B., Orosz, G., and Stepan, G. (2023b). Guided control of a human driver via an automated vehicle. *IFAC-PapersOnLine*, 56(2), 899–904.
- Szaksz, B., Orosz, G., and Stepan, G. (2025). Spectral submanifolds in time delay systems. *Nonlinear Dynamics*, published online. doi:10.1007/s11071-025-10902-0.